Chapter 4

Trialkoxysilane-functionalized synthesis of mesoporous supported palladium-nickel nanocatalyst for selective hydrazine decomposition and sensing.

4.1. Introduction

Although hydrogen is considered to be a clean fuel (Rand and Dell, 2008; Bavykin et al., 2008; Eberle et al., 2009; Jain et al., 2009; Winter et al., 2009; Armaroli et al., 2011), efficient storage and utilization of hydrogen remains a challenging task. Among various hydrogen sources (Singh et al., 2013), hydrous hydrazine (N_2H_4), which consists of nearly 8.0 wt% of hydrogen, is liquid over a wide range of temperatures (298–343 K) and less vulnerable to explosion. As such, it is considered a promising material for chemical hydrogen storage and transportation (Jiang et al., 2010; Orimo et al., 2007; Schlapbach et al., 2001; Yadav et al., 2012). Hydrous hydrazine releases gaseous products on complete decomposition [H2NNH2 -> N2 (g) + 2H2 (g)]. Partial decomposition releases NH3 along with N2 (g). There is a need for selective catalysts that enable on-board generation of hydrogen gas from hydrazine. Catalyst-enabled liberation of hydrogen on the decomposition of hydrazine has been reported over the past decade (Zheng et al., 2005; Singh et al., 2011; Song et al., 2010). Several catalysts have been studied for the decomposition of hydrazine, including nanoscale-supported catalysts (e.g., FeNi/Cu, Ni (100), Ir-MWNTs) and nanoparticle catalysts (e.g., Pt-Ni (111), Rh (0), Pt (111) (Contour et al., 1972; Alberas et al., 1992; Singh et al., 2009; Greeley et al., 2006; Serrano et al., 2009; Somorjai et al., 2009; Yamauchi et al., 2009; Liu et al., 2010; Bunker et al., 2011; Agusta et al., 2010; Manukyan et al., 2014; Oliaee et al., 2016). Although these catalysts have been reported to attain 100% H_2 selectivity, many of them require harsh experimental conditions and exhibit slow rates (Singh et al., 2009). Therefore, improved catalysts are needed to achieve high H_2 selectivity along with rapid decomposition of hydrazine; these materials should exhibit high surface area to volume ratios, high levels of dispersion, and enhanced

surface atomic catalytic activity. Ni and other 3d series transition metals are often used for catalytic applications. Ni nanoparticles may undergo rapid oxidation to oxides, which makes the surface of the nanoparticle inactive (Qiao et al., 2014). Since Ni^{2+} exhibits a low electrode reduction potential, a strong reducing agent ($NaBH_4$) is used to generate Ni (0). The use of strong reducing agents facilitates the formation of aggregates. To overcome this limitation, nickel was modified with the noble metal Pd to form Ni_xPd_y bimetallic nanoparticles, which exhibited improved catalytic behaviour (Du et al., 2015). However, inconsistent results were obtained due to the long-term instability of the material, which resulted in the loss of the desired efficiency.

We report herein on the synthesis of Ni_xPd_y, in which a Functional trialkoxysilane serves as a template for stabilizing and forming the Pd-Ni bimetallic nanocrystallite. We have demonstrated the role of 3-glycidopxypropyltrimethoxysilane (3-GPTMS) and other functional alkoxysilanes (e.g., 3-aminopropyltrimethoxysilane (3-APTMS) and 2-(3,4-epoxycyclohexyl) ethyltrimethoxysilane (EETMS)) in the synthesis and stabilization of noble metal nanoparticles and the conversion of noble metal cations to zero-valent species in the presence of various organic reducing agents (Pandey et al., 2014c; Pandey et al., 2016c). Accordingly, we prepared monometallic Pd and bimetallic Ni_xPd_y analogues with Ni and Pd in various molar ratios (e.g., 1:1, 5:1) within a mesoporous support; this approach involved Functional trialkoxysilane-mediated incorporation of palladium nanoparticles within mesopores and stabilization of the Ni-Pd nanocatalyst within the mesopores. Mesoporous silica nanoparticles (MSNPs) may be used to enhance the active surface area available for catalytic applications. We previously reported on the processing of Pd-nanoparticle-encapsulated silica-

alginate beads (Pandey et al., 2017). However, the incorporation of Ni along with Pd was not found to be compatible with this support material. Accordingly, attempts have been made to utilize other porous matrices for the assembly of Ni-Pd nanocatalysts.

The current study evaluates mesoporous silica nanoparticle-assembled nickel-palladium bimetallic nanocrystallites for catalytic decomposition of hydrous hydrazine. Functional trialkoxysilane (e.g., 3-APTMS and 3-GPTMS) facilitated the synthesis of functional noble metal nanoparticles within one minute. The decomposition of hydrous hydrazine was monitored using resonance Rayleigh scattering intensity measurements (El Kurdi and Patra, 2018). The resonance Rayleigh scattering signal of the trialkoxysilane-functionalized gold nanoparticles was monitored by synchronous fluorescence spectroscopy and was found to be linearly dependent on the concentration of hydrous hydrazine. The Pd-Ni bimetallic nanocrystallites inserted within mesoporous silica nanoparticles were shown to mediate the selective decomposition of hydrous hydrazine.

4.2. Experimental section

4.2.1. Materials and reagents

3-APTMS, 3-GPTMS tetrachloropalladate (K_2PdCl_4), formaldehyde, sodium borohydride ($NaBH_4$) ethylene glycol, and methanol were obtained from Sigma Aldrich (Bengaluru, India). Nickel chloride hexahydrate (was obtained from Himedia (Mumbai, India); all of the experiments were performed using double-distilled water.

4.2.2. Instrumentation

The as-synthesized bimetallic nanocrystallite inserted MSNPs and monometallic nanoparticles were characterized using Hitachi 800 and 8100 high-resolution transmission electron microscopes (Hitachi, Tokyo, Japan) with an acceleration voltage of 200 kV. The samples were diluted with double distilled water and ultra-sonicated for 15 min before they were placed over a carbon-coated grid. The degradation of hydrous hydrazine was monitored using a Hitachi U-2900 UV-Vis spectrophotometer (Hitachi, Tokyo, Japan). 2D and 3D fluorescence data were measured using a Hitachi F7000 instrument (Hitachi, Tokyo, Japan). Synchronous fluorescence spectroscopy using gold nanoparticles was performed using a Hitachi F7000 fluorescence spectrophotometer (Hitachi Tokyo, Japan). The excitation source used in the study was a 100 W Xenon lamp; the detector used in the study was an R-928 instrument operating at a voltage of 950 V; the excitation and emission slits were maintained at a width of 5 nm. The wavelength interval was maintained at $\Delta\lambda = 0$ nm. The collected 5 μL of Au nanoparticles were mixed with 2 mL of water and placed in a fluorescence cuvette.

4.2.3. Synthesis of AuNPs-1

3-APTMS (0.025 M in ethylene glycol) was placed in a 5 mL glass vial, followed by the addition of a methanolic solution of tetrachloroauric acid (HAuCl$_4$) (40 mM). The reaction mixture was stirred on a cyclo vertex mixture for 1 minute, followed by the addition of 3-GPTMS (3.5 M in ethylene glycol), the reaction mixture was thoroughly mixed on a cyclo vertex for 2 minutes. After that, the reaction mixture was kept in a microwave oven for 10 s.

The microwave cycle was repeated four to six times, resulting in the synthesis of dark red-colored AuNPs-1.

4.2.4. Synthesis of AuNPs-2

3-APTMS (0.025 M in ethylene glycol) was placed in a 5 mL glass vial, followed by the addition of a methanolic solution of tetrachloroauric acid (HAuCl₄) (40 mM). The reaction mixture was stirred on a cyclo vertex mixture for 1 minute, followed by the addition of 3-GPTMS (1.5 M in ethylene glycol), the reaction mixture was thoroughly mixed on a cyclo vertex for 2 minutes. After that, the reaction mixture was kept in a microwave oven for 10 s. The microwave cycle was repeated four to six times, resulting in the synthesis of dark red-colored AuNPs-2.

4.2.5. Functional trialkoxysilane mediated synthetic incorporation of palladium nanoparticles within mesoporous silica and mesoporous silica nanoparticles

MSNPs that exhibited an average size of 200 nm were made as described earlier (Singh et al.,2009). MSNPs (0.05 g) were suspended in 500 μL of 20 mM tetrachloropalladate solution in ethylene glycol under stirring for 5 h, followed by collection of palladium cation dispersed MSNPs by centrifugation. Palladium cation-dispersed MSNPs were suspended in a 3-APTMS solution (4 M) in ethylene glycol under stirring for 4 h, followed by the addition of 200 μL of 10% (w/v) formaldehyde in ethylene glycol under stirring and microwave incubation for 55 s. The PdNP-inserted MSNPs was collected from the black-colored suspension by centrifugation followed by washing with water 2-5 times to remove any unbound palladium with MSNPs.

PdNP-inserted MSNPs were dried under vacuum at 80°C for 2 h. A similar procedure was used for making PdNPs inserted mesoporous silica (pore size 6 nm and particle diameter 50 μm.

4.2.6. Synthesis of Pd-Ni NPs-1 and Pd-Ni NPs-2 bimetallic nanoparticle inserted MSNPs

0.05 g of PdNP inserted MSNPs were suspended in an aqueous solution of 20 mM nickel sulfate containing 1 % polyvinylpyrrolidone (PVP) under stirring, followed by addition of a 10 mM $NaBH_4$ aqueous solution under stirring for 30 minutes, resulting in the formation of Pd-Ni NPs-1 (Pd-Ni metal ratio 1:1) inserted MSNPs, which were collected by centrifugation. Pd-Ni inserted MSNPs were washed with water and dried in a vacuum oven at 80°C for 1 h. Pd-Ni NPs-2 (Pd-Ni metal ratio 1:5) inserted MSNPs were made using a similar process; in this case, the concentration of nickel sulfate containing 1 % PVP was 100 mM. An analogous procedure was adopted for inserting Pd-Ni NPs-1 and Pd-Ni NPs-2 within mesoporous silica a (pore size 6 nm and particles diameter 50 μm).

4.2.7. Hydrous hydrazine decomposition

The effect of different compositions of Pd-Ni inserted mesoporous silica nanoparticles on the decomposition of hydrous hydrazine were studied. The experiments were performed in four different flask reactors, which were initially filled with 2 mL of 1.19 M hydrazine aqueous solution. Approximately 5 mg of Pd-Ni inserted MSNPs was placed in the reactors. Equal volumes of aliquots were withdrawn from the reaction mixtures at regular intervals and were analyzed by resonance Rayleigh scattering.

4.3. Results and discussion

4.3.1. Microwave-assisted 3-APTMS and 3-GPTMS mediated controlled synthesis of gold nanoparticles

Trialkoxysilane mediated controlled conversion of noble metal cations into their respective nanoparticles has been demonstrated by Pandey et al., 2014. During nanoparticle formation, 3-aminopropyltrimethoxysilane acted as a Lewis base that facilitated interactions with metal cations and served as a stabilizer for metal nanoparticles. 3-APTMS treated metal cations initiated opening of the epoxide ring of 3-GPTMS forming a covalent linkage with the nitrogen of the organoamine linked to the trialkoxysilane; this process resulted in the reduction and stabilization of the metal cations. This approach enabled the functional trialkoxysilane-mediated synthesis of noble metal nanoparticles. This reaction scheme also enables bimetallic and trimetallic noble metal nanoparticles to be formed. In this study, we used two different concentrations of 3-GPTMS, 3.5 M and 1.5 M, and kept the concentration of 3-APTMS (0.040 M) constant to make gold nanoparticles of two sizes. Transmission electron microscopy and respective electron diffraction pattern data from the two different sized gold nanoparticles are shown in (Fig.4.1a, b and d, e). The average particle size of AuNPs-1 was found to be 8 nm and the average particle size of AuNPs-2 was found to be 13 nm, which is shown in Fig. 4.1c and Fig. 4.1f, respectively.
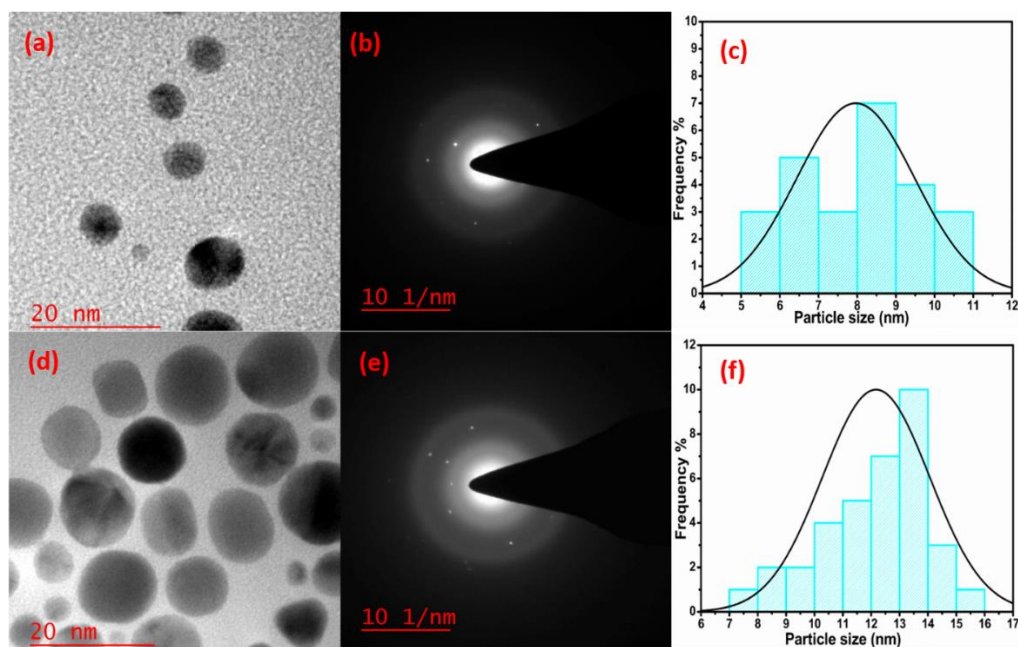
Fig. 4.1. TEM images and SAED patterns of AuNPs-1(a, b) and AuNPs-2 (d, e), respectively. The particle size distribution for AuNPs-1 and AuNPs-2 are shown in Fig. 4.1c and Fig. 4.1f, respectively.
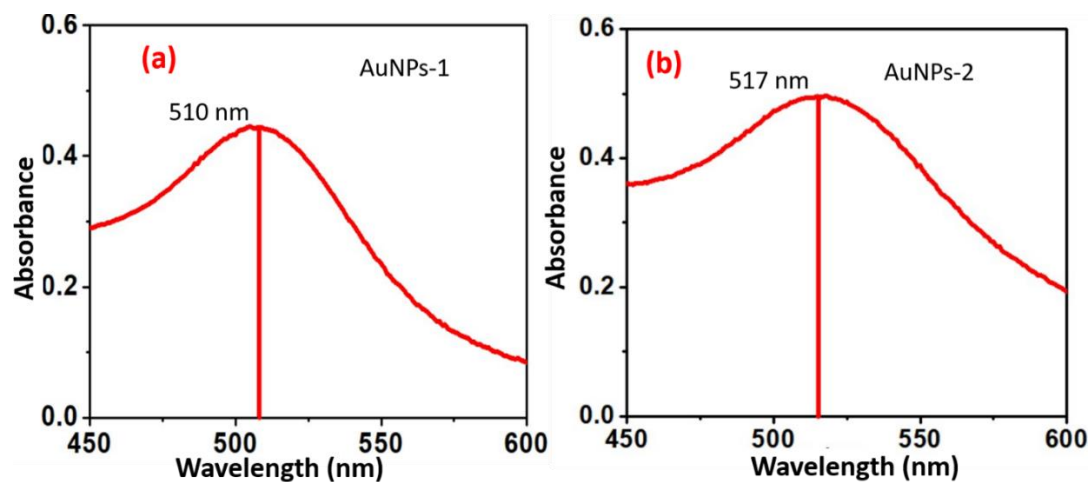

Fig. 4.2. (a) and (b) show the UV-VIS spectra of AuNPs-1 and AuNPs-2, respectively.

The absorbance maxima of AuNPs-1 and AuNPs-2 were found to be on the order of 510 nm and 517 nm, respectively; are shown in Fig. 4.2a and Fig. 4.2b.

4.3.2. Synchronous fluorescence spectroscopy of Functional trialkoxysilane-functionalized gold nanoparticles in hydrous hydrazine sensing

Synchronous fluorescence spectroscopy has found extensive use in the identification and quantitative analysis of compounds in solution (Samokhvalov et al., 2020; Du et al., 2015). These efforts directed us to examine the role of gold nanoparticles in hydrous hydrazine detection. The resonance Rayleigh scattering of gold nanoparticles as monitored by synchronous fluorescence spectroscopy was shown to be potentially useful for the detection of hydrous hydrazine; the interaction between the gold nanoparticles and the analyte alters the synchronous fluorescence spectroscopy signal as a function of analyte concentrations. Fig. 4.3a shows the synchronous fluorescence spectra recorded with AuNPs-1 at $\Delta\lambda = 0$ nm in the absence and the presence of hydrous hydrazine of different concentrations. The results predict a significant increase in synchronous fluorescence spectroscopy intensity as a function of the hydrous hydrazine concentration. Fig. 4.3b indicates a linear relationship between the synchronous fluorescence spectroscopy signal and the hydrous hydrazine concentration. The effect of gold nanoparticle size on the synchronous fluorescence spectroscopy signal was evaluated using AuNPs-2. Data collected with 8 nm gold nanoparticles is shown in Fig. 4.3a and b, data collected with 12 nm gold nanoparticles is shown in Fig. 4.3c and d.
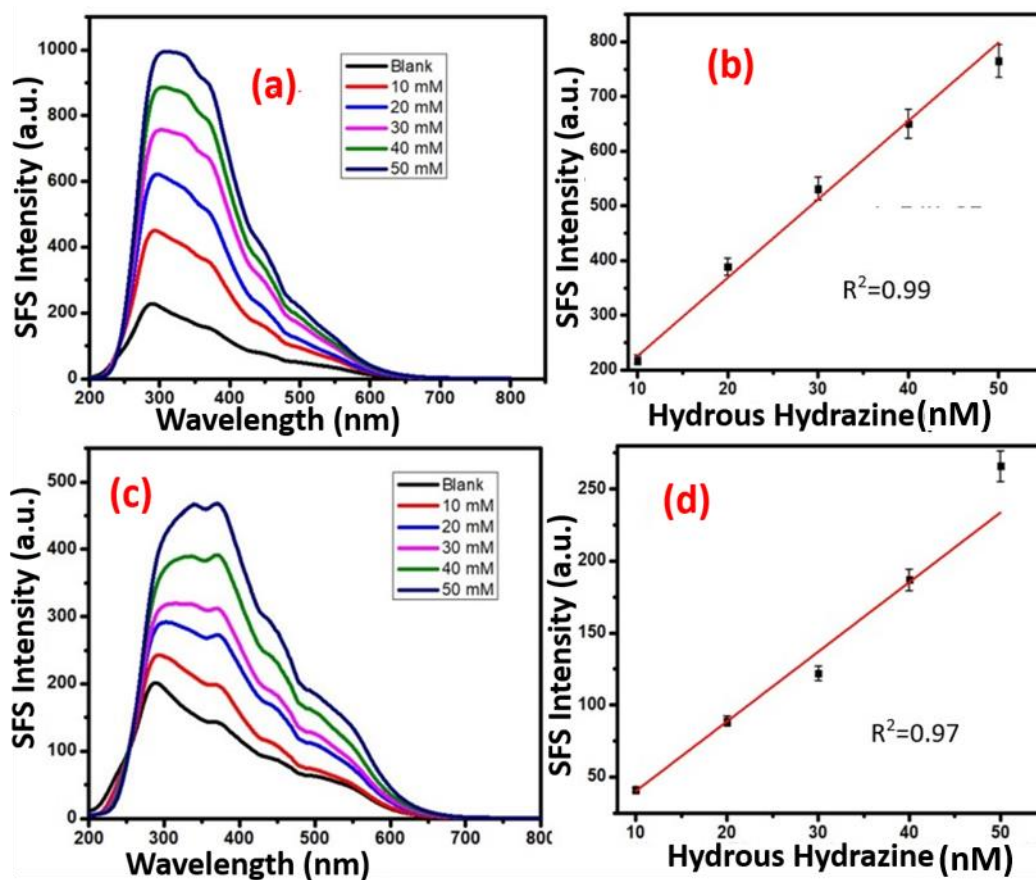
Fig. 4.3. (a) and (c) show the synchronous fluorescence spectra at delta $\Delta\lambda=0$ recorded in the absence and the presence of different concentrations of hydrous hydrazine of AuNPs-1 and AuNPs-2, respectively. (c) and (d) show the synchronous fluorescence spectrum intensity versus hydrous hydrazine concentration for AuNPs-1 and AuNPs-2, respectively.

The results as shown in (Fig. 4.3 a-d) indicate the dependence of the synchronous fluorescence spectroscopy signal on the gold nanoparticle size. It should be noted that the extent of the change in the synchronous fluorescence spectroscopy signal with AuNPs-2 (Fig. 4.3c) was found to be considerably less than that with AuNPs-1 (Fig. 4.3a) under similar

conditions. This finding indicates that the synchronous fluorescence spectroscopy signal is a function of gold nanoparticle size. The results shown in Fig. 4.3 indicate that the presence of hydrous hydrazine can be monitored using the synchronous fluorescence spectroscopy signal recorded from AuNPs, this approach is utilized to detect Pd-Ni mediated hydrous hydrazine decomposition.

The findings as shown in (Fig. 4.1-4.3) indicate that an increase in the 3-APTMS concentration during gold nanoparticle synthesis was associated with an increase in the size of the gold nanoparticles. On the other hand, under similar conditions, an increase in 3-GPTMS concentration at a constant 3-APTMS concentration was associated with a decrease in the size of the gold nanoparticles. Accordingly, decreasing the concentration of 3-APTMS while increasing the concentration of 3-GPTMS during functional trialkoxysilane-mediated synthesis of nanoparticles could be explored for making gold nanoparticles for the detection of hydrazine based on synchronous fluorescence spectroscopy measurements.

4.3.3. Synthesis and characterization of Pd-Ni bimetallic nanocrystallite inserted mesoporous silica nanoparticles

The functional trialkoxysilane over the mesoporous silica support provides a template for the incorporation of nanoparticles within the mesoporous matrix via the self-assembly of silanol residues. Accordingly, functional trialkoxysilane-mediated formation of palladium nanoparticles was used to create the Pd-Ni bimetallic nanocrystallites. During the synthetic insertion of PdNPs within the mesoporous support, the palladium cations were allowed to distribute within the mesopores under stirring, followed by the collection of the palladium

cation-inserted mesoporous support through centrifugation. The palladium cation-inserted mesoporous support was then allowed to interact with 3-APTMS under stirring, followed by the addition of either 3-GPTMS or formaldehyde, which served as the reducing agent for the 3-APTMS treated palladium cations. Microwave incubation for less than 1 minute caused a rapid formation of the PdNP-inserted mesoporous support, which was collected by centrifugation, washed with water, and dried at 80 °C.

To prepare the Pd-Ni NPs inserted mesoporous support, the PdNP inserted MSNPs were suspended in a PVP-stabilized aqueous solution of nickel sulfate, which enabled the reduction of Ni cations by sodium borohydride. The use of 3-APTMS and 3-GPTMS provided an excellent template for yielding Pd-Ni bimetallic nanocrystallites within the mesoporous support.
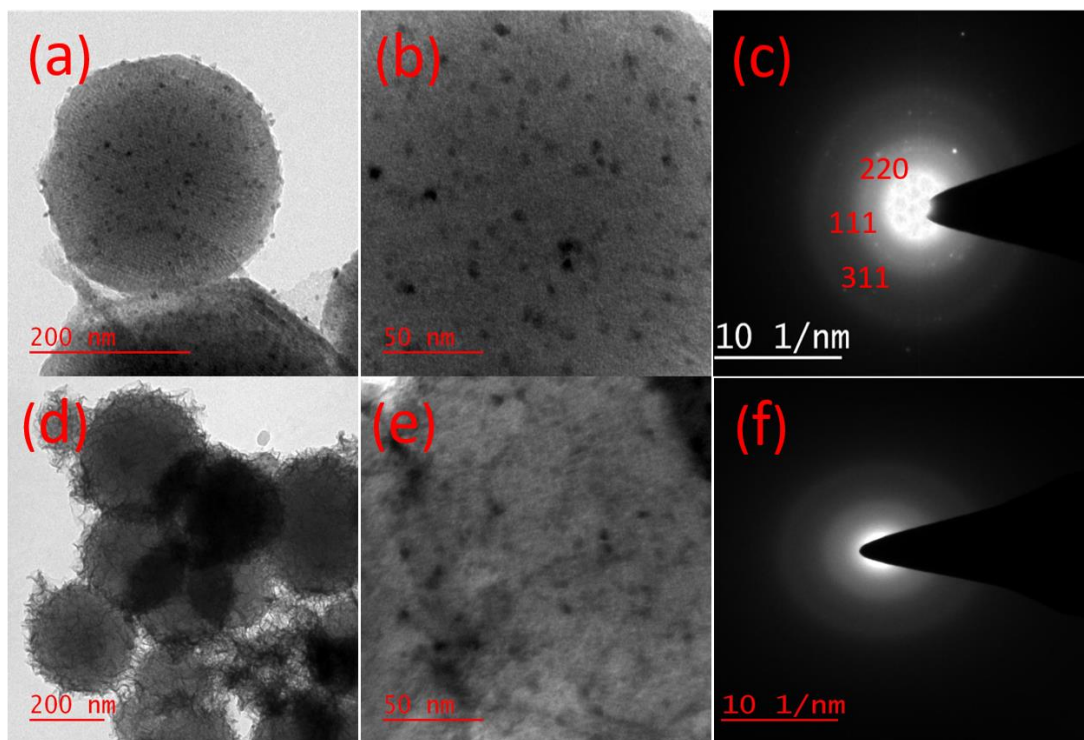
Fig. 4.4**.** TEM images and SAED patterns of Pd-Ni NPs-1 are shown (a, b, and c), and for Pd-Ni NPs-2 (d, e, and f) inserted mesoporous silica nanoparticles, respectively.

The transmission electron microscopy imaging (TEM) of the nanocrystallites with as-prepared Pd-Ni NPs-1 and Pd-Ni NPs-2 inserted nanocrystallites, is shown in Fig.4.4. TEM images and a selected area electron diffraction pattern (SAED) of Pd-Ni NPs-1 inserted MSNPs are shown in Fig. 4.4 (a-c). The planes confirm the presence of both Pd and Ni components of the bimetallic nanocrystallites within mesoporous silica nanoparticles. Fig. 4.4 a, b, suggests that the average size of Pd-Ni NPs-1 nanocrystallites was found to be on the order of 4 nm. Fig. 4.4 (d-f) shows the TEM images and selected area electron diffraction pattern (SAED) of Pd-Ni NPs-2. The average size of the Pd-Ni NPs-2 nanocrystallites was

found to be on the order of 6 nm. These findings indicate that functional trialkoxysilane enabled

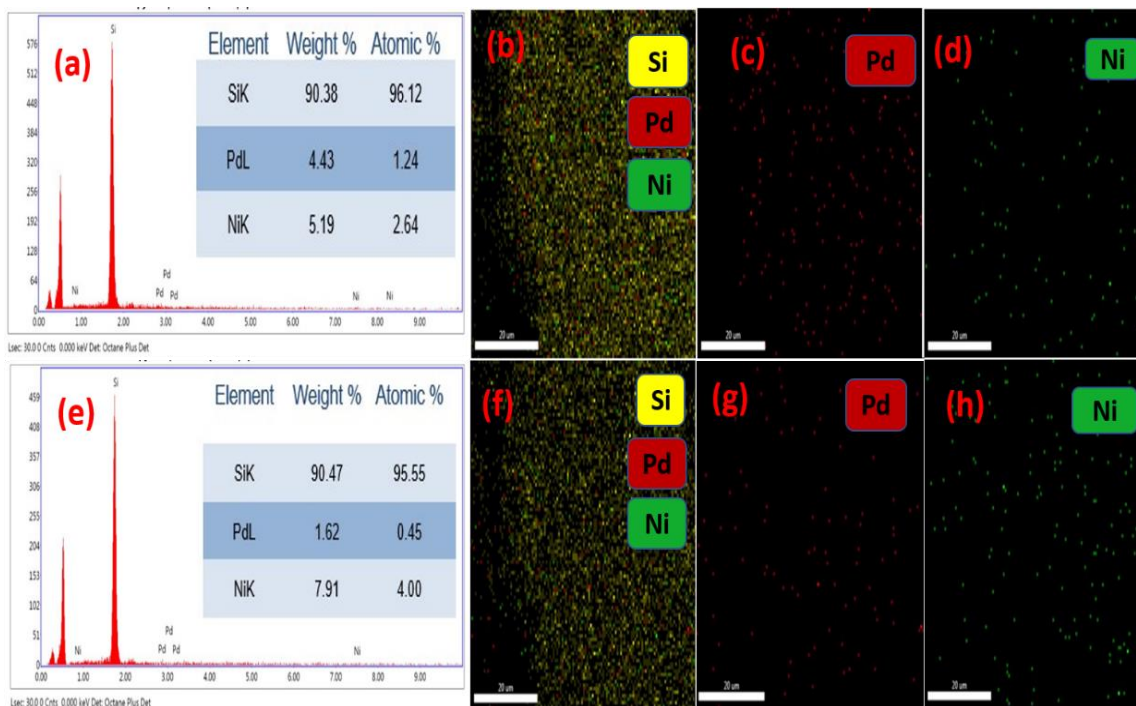controlled formation of Pd-Ni bimetallic nanocrystallites within the mesoporous matrix.

Fig. 4.5. (a) and (e) show the EDX results of bimetallic Pd-Ni NPs-1 inserted MSNPs and Pd-Ni NPs-2 inserted MSNPs, respectively. (b-d) and (f-h) show the elemental mapping of Pd-Ni NPs-1 and Pd-Ni NPs-2 inserted MSNPs respectively.

The energy dispersive X-ray (EDX) and elemental mapping of Pd-Ni at two different ratios are shown in Fig. 4.5. The EDX results of Pd-Ni NPs-1 and Pd-Ni NPs-2 are shown in Fig. 4.5a and Fig. 4.5e, respectively. Elemental mapping of Pd-Ni NPs-1 and Pd-Ni NPs-2 is shown in Fig. 4.5 (b-d) and Fig. 4.5 (f-h) respectively. These findings confirm the presence of the desired metal in functional trialkoxysilane mediated synthetic incorporation of nanocrystalline within the mesoporous support.
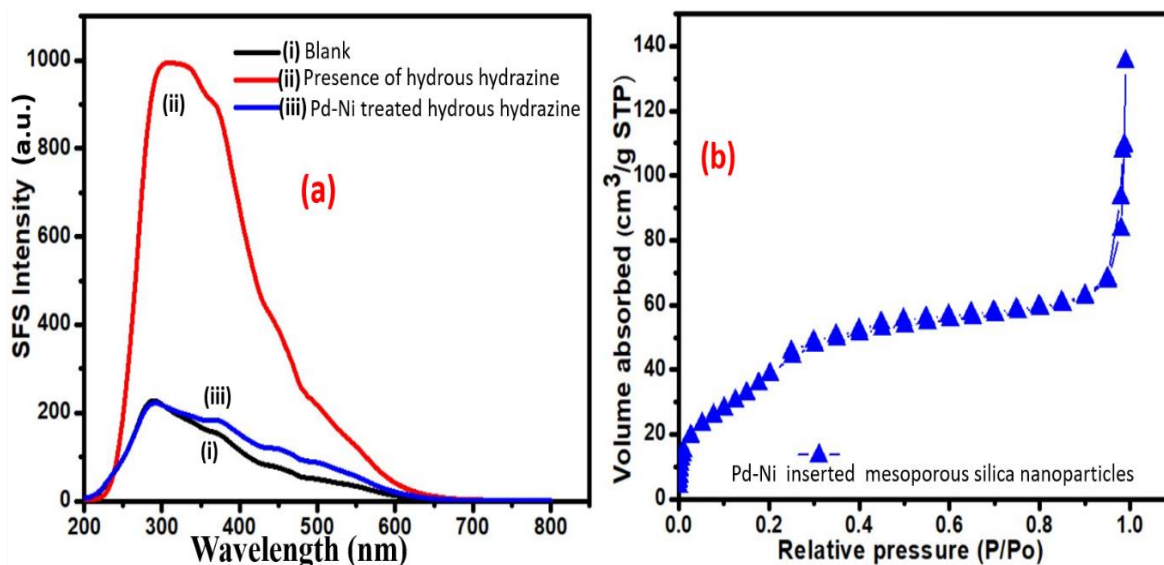
4.3.4. Decomposition of hydrous hydrazine

Fig. 4.6. (a)Synchronous fluorescence spectra at delta $\Delta\lambda=0$ nm recorded before (ii) and after (iii) hydrous hydrazine decomposition; (i) shows the control. (b) N_2 adsorption-desorption isotherms of Pd-Ni NPs-1 inserted mesoporous silica nanoparticles.

Nanocatalyst	Specific BET surface m^2g^{-1}	Pore volume cm^2g^{-1}	Average pore diameter (nm)
Pd-Ni NPs-1 inserted MSNPs	177	0.151	4.68

Table 4.1. show the data on specific surface area, pore volume and average pore diameter of Pd-Ni inserted mesoporous support.

The decomposition of hydrous hydrazine over Pd-Ni inserted MSNPs was studied. 10 mg of the nanocatalyst-inserted mesoporous support was shown to induce decomposition of 3 mL hydrous hydrazine (1.2 M) at room temperature (25°C) under stirring.

The decomposition of the hydrous hydrazine was monitored by detecting it before and after the addition of the nanocatalyst via monitoring of the synchronous fluorescence spectroscopy signal intensity (Fig. 4.6a). After 45 minutes of incubation, complete decomposition of hydrazine was recorded as confirmed from Fig. 4.6a (ii) and (iii), this result confirming the potent efficiency of the functional trialkoxysilane stabilized Pd-Ni NPs-1 nanocrystallite within the MSNPs support. Nanocrystallite Pd-Ni NPs-1 (with a metal ratio of 1:1) exhibits greater activity for the decomposition of hydrous hydrazine than Pd-Ni NPs-2 (with a metal ratio of 1:5). At higher concentrations, Nickel converts into Nickel oxide, which explains how it was that Pd-Ni does not exhibit greater activity for hydrous hydrazine decomposition.

The catalytic activity of the as made nanocatalyst was compared with those reported earlier (Chen et al., 2017), for example, Chen et al. described a Pd-Ni/ reduced graphene oxide catalyst that enabled only 67% decomposition of hydrazine in 60 minutes at 30°C. These results revealed the excellent catalytic activity of the as- made highly stable mesoporous supported Pd-Ni nanocatalyst for catalytic applications.

The nitrogen adsorption-desorption isotherms of Pd-Ni NPs-1 inserted MSNPs are shown in Fig. 4.6b. This nanocatalyst exhibits a type II isotherm, resulting from the capillary

condensation of nitrogen in the porous matrix. The Pd-Ni Nps-1 inserted mesoporous silica nanoparticles displayed a relative pressure of 0.25-0.7, which indicated that the average pore diameter was on the order of 3.59 nm. The specific BET surface area, pore volume and average pore diameter are shown in the insert of Table 4.1.

4.4. Conclusions

To summarize, we have reported on a novel approach to fabricate Functional trialkoxysilane-stabilized noble metal nanoparticles and their bimetallic analogues. Functional trialkoxysilane enabled the synthetic insertion of Pd-Ni bimetallic nanocrystallites within mesoporous silica nanoparticles. Functional trialkoxysilane-stabilized gold nanoparticles showed hydrous hydrazine concentration-dependent signals from resonance Rayleigh scattering; this approach was used to detect hydrous hydrazine and the extent of Pd-Ni catalyzed decomposition of the same. The Pd-Ni inserted mesoporous silica nanoparticles enabled complete decomposition of the hydrous hydrazine into hydrogen and nitrogen at room temperature (30 $^\circ$C), as such, the material may serve as a catalyst for the hydrogen evolution reaction.